Mechatronics 32 (2015) 59–66

Contents lists available at ScienceDirect

Mechatronics

journal homepage: www.elsevier.com/locate/mechatronics

Performance study on a novel variable area robotic fin

Bo Liu[a,b], Yikun Yang[a], Fenghua Qin[c], Shiwu Zhang[a,*]

[a] Department of Precision Machinery and Precision Instrumentation, University of Science and Technology of China, Hefei, Anhui 230027, China
[b] Institute of Systems Engineering, China Academy of Engineering Physics, Mianyang, Sichuan 621999, China
[c] Department of Modern Mechanics, University of Science and Technology of China, Hefei, Anhui 230027, China

ARTICLE INFO

Article history:
Received 9 February 2015
Accepted 12 October 2015
Available online 3 November 2015

Keywords:
Variable area robotic fin
Thrust force
Efficiency
Control modes

ABSTRACT

Fish fin possesses large deformations in its motion cycle assisting fish's swimming, in which its geometric parameters such as surface area, aspect ratio change greatly, and the complex deformations and motions result in complicated hydrodynamic response. In this paper, the dynamic change of surface area is concentrated to improve the propulsion performance of underwater propeller. A novel variable area robotic fin is developed and the effect of surface area change on the hydrodynamic forces is investigated quantitatively. The robotic fin composes two parts: a base fin with hand shaped holes and a cover fin that fits the shape of the holes. The change of the surface area of the robotic fin is realized by rotating the cover fin to shield the holes in the base fin. A crank-rocker-cam composite mechanism is designed to realize the fin pitching motion and surface change motion synchronously with one driving motor. Four control modes of surface area change in a motion circle are investigated, namely, complete traditional invariable fin, traditional invariable fin with smaller surface, fin with larger surface during in-strokes and fin with larger surface during out-strokes. The thrust force and efficiency of the four control modes with various swimming speeds are detailed experimented and discussed. It is found that the variable area fin achieves a remarkable different hydrodynamic response and the corresponding control modes affect much. For the variable surface area fin, they generate average thrust force between the complete invariable fin and invariable fin with smaller surface, in which the fin with larger surface area during in-strokes follows closely the complete traditional invariable fin, while the fin with larger surface area during out-strokes performs more like the traditional invariable fin with smaller surface. It is interesting that fin with larger surface during in-strokes can generate much larger average thrust force than the fin with large surface during out-strokes. For the efficiency, the fin with larger surface during in-strokes behaves the best. And the effect of the surface area change ratio and time is closely connected with the control modes. Besides, the influences of pitching frequency and amplitude are also studied. The results demonstrate that the propulsive performance can be indeed improved by proper surface area change in a motion cycle, which will be an inspiration to the design of novel underwater robot propulsive system.

1. Introduction

Fish has fascinated researchers for their remarkable swimming talent with efficiency, speed, and agility for recent years, which has inspired a variety of research ranging from theoretical study on swimming features to robotic fish developing [1–5]. After the longtime of evolution to perfectly adapt to the underwater environment, the fins become vital in the swimming movement for most of the fish. The caudal fin acts as dominant propeller with the pectoral fin, dorsal fin and other fins assisting in the Body and/or Caudal Fin (BCF) modes, while the pectoral fin is the main propeller for the Median and/or Paired Fin (MPF) modes, the dorsal fin and anal fin may be used to assist the body position and stability in the motion [6,7]. Since their prominent and multiple roles in fish propulsion and maneuvering, abundant studies on the fins have been conducted including physiology, morphology and kinematic to study the fins' structure and swimming performance [8–12], to assist the development of robotic fins [13–15].

In recent years, the three-dimensional complex motions of fish fins have attracted researchers' attention and their hydrodynamic forces are intensively studied. Lauder *et al.* studied the highly deformable pectoral fin of bluegill sunfish during steady forward swimming [16,17], Flammang studied the caudal fin deformation of blue gill sunfish in maneuvering motions [18]. They found out that the fins exhibit complicated forms whether in cruising movement or maneuvering movement which may be caused by active control of the fin ray or the passive deformation because of the fin flexibility. To explore the three-dimensional motion, Bozkurttas *et al.* extracted

* Corresponding author. Tel.: +86551-63600249.
E-mail address: swzhang@ustc.edu.cn (S. Zhang).

http://dx.doi.org/10.1016/j.mechatronics.2015.10.004
0957-4158/

several motion modes by proper orthogonal decomposition (POD) such as "cupping", "expansion" which can describe the complex kinematics of pectoral fin of sunfish [19]. In the study on the pectoral fin of Koi Carp [20], the fin ray motions was extracted, and the highly deformable motions of the fin ray in a motion cycle were reconstructed. Based on these study, researchers have developed various robotic fins. Tangorra *et al.* designed bio-robotic fish fins with several moveable fin rays which can be controlled to generate complex conformations and studied their hydrodynamic response [21,22]. Their pectoral or caudal fin can closely mimic the three-dimensional motions and the fin's flexibilities are evaluated. Zhang *et al.* also developed a robotic pectoral fin with shape memory alloy (SMA) in which the fin can realize some basic motions such as "cupping" and "expanding" [23].

Though many studies on the complex 3D motions and their comprehensive hydrodynamic forces of the fins have been conducted, little attention has been paid on the detailed surface shape change of fins and their effects on the hydrodynamic response quantitatively. For example, the fin conducts complex deformations in a motion cycle, the deformations lead to the change of effective flapping surface area, the equivalent aspect ratio, the sweepback and so on. How do these parameters change? What are these changes' effects on the forces, especially in a dynamic motion cycle? A few studies have been conducted on these changes. The deformation is a complicated process, and it would be a tough work to analyze all the parameters together quantitatively. We first take the flapping surface area change into consideration since it possesses notable changes in either "cupping" motion, "waving" motion or "expanding" motion. In [20], we calculated the surface area change in hovering and retreating by digital image processing. The surface area shows a considerable change in a period and reaches up to 1.4 (with 560 /400 mm^2) which indicates that the surface area change may profit the propulsive performance. In this paper, we focus on the influence of variable surface area on propulsive performance and develop a variable area robotic fin, which can vary its area in a dynamic motion cycle. We then conduct plenty of experiments to explore its hydrodynamic response quantitatively.

The reminder of the paper is organized as follows: in Section 2, the design concept of the robotic fin and driving module are introduced, the control strategy of the surface area change is also presented. In Section 3, the detailed manufacturing and realization of the fin and experimental system are exhibited. Then in Section 4, experiments of various control modes and kinematic parameters are conducted, their thrust forces and efficiency are detailed presented and discussed. Section 5 concludes the paper.

2. Variable area robotic fin system

As presented in [16,17,19,20], the fish fin possesses great deformations in a motion cycle, its geometric parameters vary dynamically. Its contours, the aspect ratio (which is defined as span-wise length versus chord-wise length) and the flapping surface area vary much in such a transient cycle because of the three-dimensional motions such as "cupping" and "undulation". These changes affect the hydrodynamic forces and assist fish cruising or maneuvering. In this paper, the change of flapping surface area is taken into consideration.

2.1. Variable area robotic fin

To realize the change of surface area with other geometric parameters such as aspect ratio, appearance contours fixed, we design a robotic fin as shown in Fig. 1. The robotic fin composes two parts: a base fin with holes and a cover fin that fits the shape of the holes. The base fin is simplified into a fan shaped model, on which several holes are punched. These holes are arranged similar to hand shape, and they occupy the same size with the ridges. The cover fin also possesses the same size with the holes. When the cover fin is driven to rotate around the axis on the base fin, it can cover or uncover the holes exactly. In this way, the robotic fin's surface area is changed.

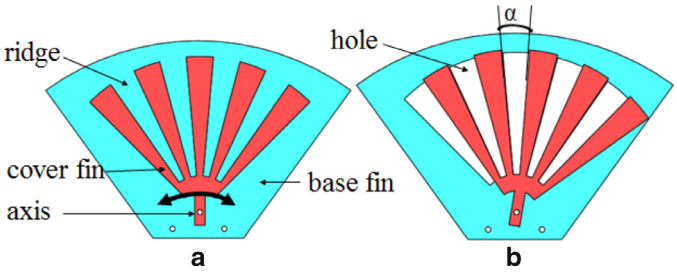

Fig. 1. Variable area robotic fin: base fin (sky blue colour) and cover fin (red colour): (a) cover fin covers the holes in the fin model; (b) cover fin is driven to rotate around the axis to cover the ridges, so the holes in the base fin is uncovered. (For interpretation of the references to colour in this figure legend, the reader is referred to the web version of this article).

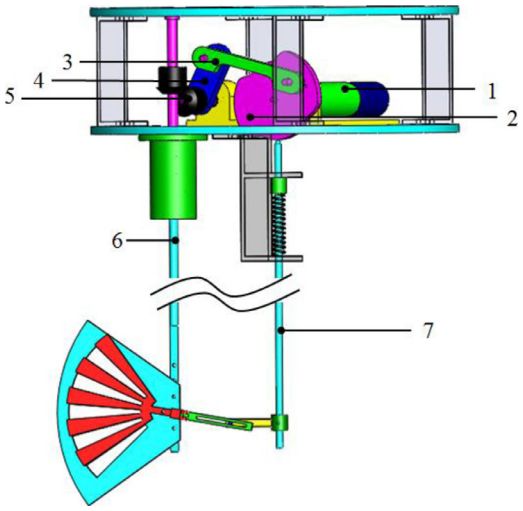

Fig. 2. Sketch of the driving module. 1. motor, 2. crank-cam, 3. middle rod, 4. rocker, 5. bevel gear, 6. pitching rod, 7. slide rod.

Hand shaped separate holes rather than a big square hole are adopted because the former one can realize a larger changing ratio of the surface area with a relatively smaller rotation angle.

2.2. Driving module of the robotic fin

We apply a pitching motion on the robotic fin during propulsion, so there are two motions for the robotic fin to achieve synchronously, namely, pitching motion and surface area change motion. We propose a crank-rocker-cam composite mechanism to realize the two motions synchronously with one driving motor as shown in Fig. 2, in which the crank and the cam are integrated into component (2).

For the pitching motion, the motor (1) drives the crank-rocker system (2-3-4) to move, the rotation motion of the motor (1) is transferred into a swinging motion of the crank (4). By the bevel gear set (5), the swinging motion changes direction, then through the pitching rod (6), the robotic fin realize the pitching motion. For the surface area change motion, the motor (1) drives the cam-slide rod (2–7) to move, the designed cam drives the slide rod (7) ups and downs, which then drives the cover fin rotates around its axis through several connecting rod. The cover fin's rotating angle and time reflect the surface area change ratio and time, and it is directly actuated by the slide rod, but is determined by the profile of the cam. By designing different cam profiles, we can achieve different surface area change ratios and time.

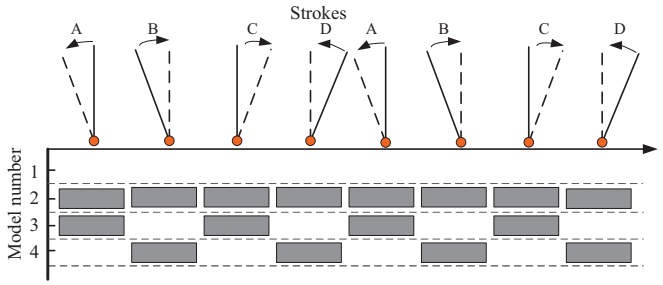

Fig. 3. Four control modes. A and C stand for out-stokes, B and D stand for in-strokes. The gray diamond stands for state "1".

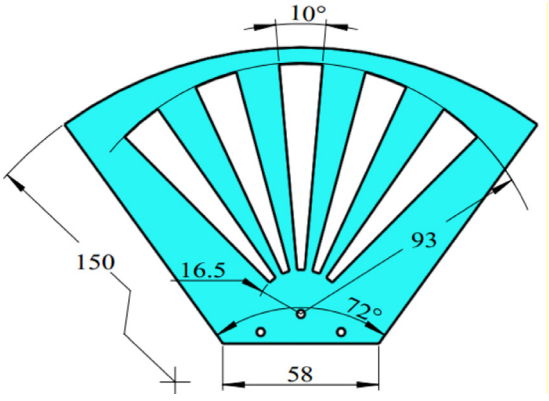

Fig. 4. Dimension of the base part of the robotic fin.

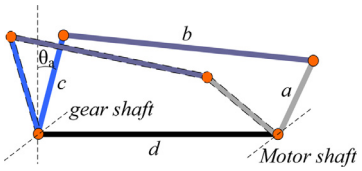

Fig. 5. Sketch of the crank-rocker structure.

Table 1
Specification of the crank-rocker mechanism.

θ_a (°)	a (mm)	b (mm)	c (mm)	d (mm)
30	20	75.9	50.6	60
45	20	64.1	30.2	60
60	20	61.3	23.6	60

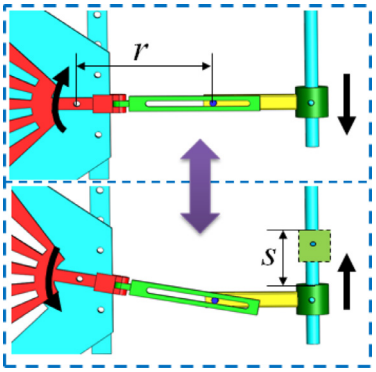

Fig. 6. Motion sketch of the cover fin.

2.3. Control modes of the robotic fin

One cycle of a pitching motion is divided into four stages, two out-strokes and two in-strokes. We also define two states for the holes in the robotic fin, the first one is defined by "0" which means the holes are fully covered, while the other one is defined by "1" which means the holes are totally uncovered.

Combing the four stages and the two states, there are total 16 control modes. Taking symmetry and practical issues into consideration, we select four modes to study as shown in Fig. 3: Mode I: 0000, Mode II: 1111, Mode III: 1010, Mode IV: 0101. Mode I means the holes are all covered during the whole motion cycle, which is opposite to Mode II whose holes are totally uncovered. Mode III means the holes are covered for the two in-strokes and uncovered for the two out-strokes which is opposite to Mode IV. Mode I represents the traditional invariable complete fish fin, Mode II represents the traditional invariable fish fin with smaller surface area, Mode III represents the fin with larger surface during in-strokes, and Mode IV represents fin with larger surface during out-strokes.

3. Manufacturing and realization of the experimental system

3.1. Manufacturing of the robotic fin

The base fin and cover fin is made of Acrylic which is very light but with enough strength, the detailed dimensions are presented in Fig. 4. The whole fin surface area is 12691 mm^2, and the surface area subtracting holes is 9300 mm^{2,} so the largest surface area change ratio can reach 1.4 with α (shown in Fig. 1) equals to 10°, the largest surface area changing ratio follows the kinematic study in [20].

3.2. Realization of the pitching motion

For the pitching motion, a sinusoidal function is adopted.

$$\theta(t) = \theta_b + \theta_a \sin(2\pi f t + \theta_i) \quad (1)$$

where $\theta(t)$ stands for the pitching angle, θ_a stands for the pitching amplitude, θ_b stands for the bias pitching angle (which is 0 in this study indicating it starts from the equilibrium position). f stands for the pitching frequency, and θ_i stands for the initial phase which is also set as 0 here.

The structure of the crank-rocker is shown in Fig. 5. *a, b, c* and *d* stand for the length of crank, middle rod, rocker, and frame as shown in Fig. 2, respectively. For the crank-rocker mechanism, considering a compact structure and no interfering of each component, we set *d* as 60 mm and *a* as 20 mm, the values of *b* and *c* are determined by the pitching amplitude θ_a as shown Fig. 5. In this paper, we investigate three pitching amplitudes, according to Eq. (2) and Fig. 5, their corresponding dimensions are listed in Table 1.

$$\begin{cases} \cos(90 - \theta_a) = \dfrac{d^2 + c^2 - (b-a)^2}{2cd} \\ \cos(90 + \theta_a) = \dfrac{d^2 + c^2 - (b+a)^2}{2cd} \end{cases} \quad (2)$$

3.3. Realization of the surface area change motion

The surface area change motion is determined by the profile of the cam. For the cam design, its lift distance (s) and lift angle (β) are the two key parameters since the lift distance is related to the cover fin rotation angle and the lift angle is related to the cover fin rotation time. Then the cover fin rotation angle reflects the surface area change ratio and the cover fin rotation time reflects the surface area change time.

Rotation angle α as shown in Fig. 1 is connected to the cam lift distance by r as shown in Fig. 6. Their relationship is defined as$s = r\sin(\alpha)$. Though r changes when the slide rod moves, it changes little. Meanwhile, α is small, so the formula is simplified to $s = r\alpha$.r is set as 40 mm according to the structure size. When the hole is totally covered, α is 10°, the corresponding lift distance is calculated with

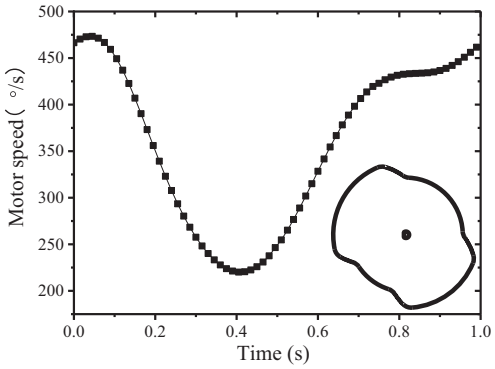

Fig. 7. An example of the designed rotation speed of the motor and profile of the cam.

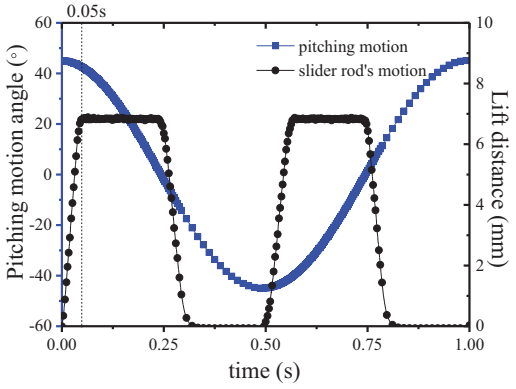

Fig. 8. Motion of the rocker and slide rod driven with the cam in Fig. 7.

the value of 7 mm. For a cam, the lift angle β could not be set as 0° since it couldn't be driven to move with a vertical slope which means the surface area change time could not reach 0. Based on the overall consideration of the cam pressure angle, the smallest lift angle is set as 20°.

In the study, we investigate the influence of different lift distances and lift angles. When the lift distance is 7 mm which means the cover fin can rotate 10°, the surface area change ratio reaches 1.4, we vary the lift distance to achieve different surface area change ratios with 1.4, 1.3, and 1.2, the corresponding lift distances are 7 mm, 5.6 mm, and 4.2 mm, respectively. The lift angle reflects the cover time of the holes, when the lift angle is 20°, it's surface area change time is 0.05 s, we vary the lift angle to achieve different surface area change time with 0.05 s, 0.1 s and 0.15 s.

3.4. Realization of the coordinated motion

Because of the quick-return characteristic of the crank-rocker mechanism, the motor speed is carefully designed to realize the fin's sinusoidal motion. Meanwhile, the cam profile is also carefully designed to realize the coordinated motions of the robotic fin. Fig. 7 presents an example of the motor speed and the profile of cam, where the pitching amplitude is 45° and the frequency is 1 Hz. The lift distance is 7 mm, which means the cover fin can rotate 10°. The lift angle is 20°, which means the cover fin will finish the rotation motion within 0.05 s at every start of the four stages. Its corresponding trajectory of pitching motion and slider rod's motion are shown in Fig. 8. By combining different cam profile and motor speed, together with the different crank-rocker dimensions, various surface area change ratios and time and kinematic cases can be realized.

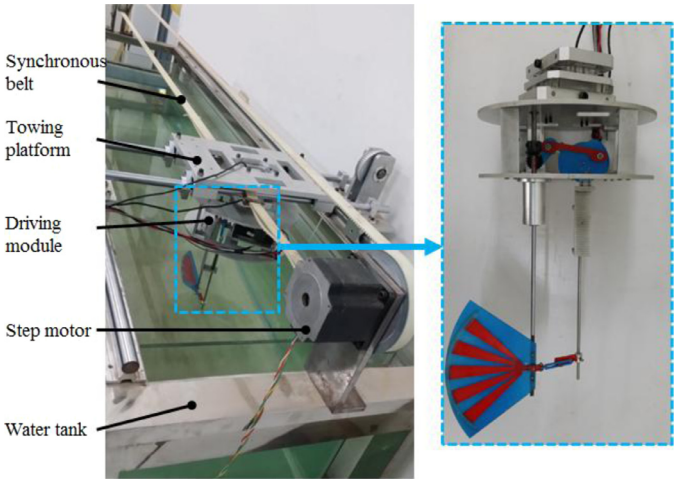

Fig. 9. Experimental setup.

3.5. Experimental system setup

Fig. 9 illustrates the whole experimental setup for the variable area robotic fin. The experiments are conducted in a transparent water tank with a size of 2 m × 1 m × 0.8 m. The driving module is connected to the towing platform by two-dimensional force transducer (JLBS-v, Jnsensor, China), which is used to measure the hydrodynamic force during the propulsion of the robotic fin. The towing platform is driven by a step motor (85BYGH, Shuangjie, China) with a speed of V to imitate the water flow. The fin is located in the middle of the water tank to avoid the interference effect from the water surface and the tank bottom.

4. Results and discussions

To investigate the effect of dynamic variable area surface on propulsive performance, the thrust force and efficiency are measured, respectively. The force is measured by the force transducers and the efficiency is defined following Lighthill [1].

$$P_u = \overline{F} \cdot V \tag{3}$$

$$P_a = \frac{\int_0^T U(t)I(t)dt}{T} \tag{4}$$

where the useful output P_u is defined by the average thrust force $\overline{F}$ and swimming speed V. In the experiments, the thrust force is defined along the swimming direction, namely along the belt direction as shown in Fig. 9. The swimming speed is imitated by the movement of the towing platform, which varies from 0 to L mm/s, L stands for the chord-wise length of the base fin which is set as 110 mm. The total power input P_a is defined by the voltage $U(t)$ and current $I(t)$ of the motor, T denotes the period of the fish fin. It should be noted that for the whole power input, the mechanism power loss P_m is included, so the pure consumption of the fin model in water P_w is obtained by subtracting the mechanical loss. P_m is also calculated by Eq. (4) where the voltage and current is obtained in air. The propulsive efficiency is defined by the useful power output and the pure power input as presented in Eq. (5).

$$\eta = \frac{P_u}{P_w} = \frac{P_u}{P_a - P_m} \tag{5}$$

Mainly four groups of experiments are conducted. In experiment 1, the thrust force and efficiency of the four control modes with various swimming speeds are investigated. In experiments 2 and 3, the surface area change ratio and time of Mode III and Mode IV are studied. In experiment 4, the pitching parameters are detailed discussed.

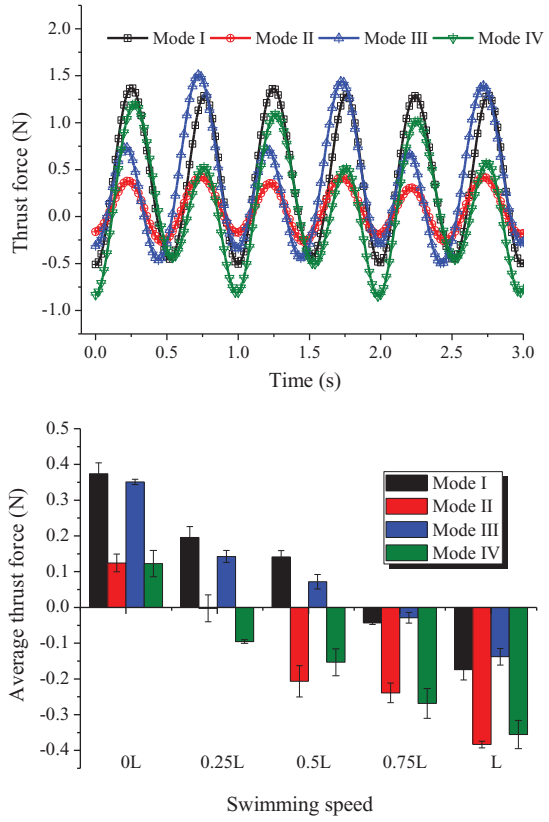

Fig. 10. Thrust force of four modes. Swimming speed is zero which means still water, (b) the average thrust force of various swimming speeds. Average values are based on five consecutive periods.

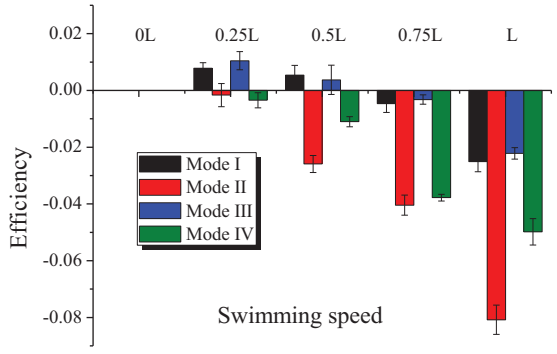

Fig. 11. Efficiency of four control modes with various swimming speeds.

Table 2
Parameters used in experiment 1.

Parameter	Specific value
Pitching frequency	1 Hz
Pitching amplitude	45°
Swimming speed	0, 0.25L, 0.5L, 0.75L, L
Surface area change ratio	1.4
Surface area change time	0.05 s

4.1. Influence of control modes

Four control modes for the fin surface change are proposed in Section 2, their thrust forces and efficiencies are detailed investigated as presented in Figs. 10 and 11. The values of parameters used in experiment are listed in Table 2.

Table 3
Parameters used in experiment 2.

Parameter	Specific value
Pitching frequency	1 Hz
Pitching amplitude	45°
Swimming speed	0.25 L
Surface area change ratio	1.4, 1.3, 1.2
Surface area change time	0.05 s

As shown in Fig. 10(a), all the thrust forces show double frequency compared with the fin motion, but their amplitudes differ much. Mode I possesses relatively larger peaks, while Mode II generates the smallest thrust force amplitude. For Mode III and Mode IV, the force is no longer symmetrical. It is seen that they generate thrust force ups and downs, the peak value and valley value vary and the largest peaks and valley achieve at different moment. Meanwhile, Mode III achieves the largest peaks while Mode IV achieves the smallest valley value. This is reasonable since for Mode I and Mode II, the pitching surface is unchangeable in the motion cycle, while it varies during the out-strokes and in-strokes for Mode III and Mode IV which leads to the force change in a motion cycle. However, it is observed that most part of the four modes forces are positive indicating all of them can generate average thrust force. The average thrust forces of different swimming speeds are shown in Fig. 10(b). It is seen that for the four modes, they can generate thrust with low swimming speeds but drag force as the swimming speed increase. However, the values differ much. The swimming speed of zero thrust force reflects the corresponding cruise speed. It is seen that Mode I can generate the largest average thrust force and largest cruise speed for all the speeds tested. Mode III follows closely and behaves better when the speed is L mm/s. Mode II and Mode IV generate less average thrust force and obtain smaller cruise speed. These two modes' performances differ little. For the two variable surface area fins' comparison, it is found out that Mode III behaves better than Mode IV and can generate much larger average thrust force.

Then the swimming efficiency is investigated as shown in Fig. 11. The negative value of efficiency means that drag force is generated. It is seen that the efficiency of all four modes decrease with the increasing of the swimming speed. Mode III namely the fin with larger surface during in-strokes performs better and can generate larger efficiency than other modes while Mode II behaves worst. The results are valuable which means the fin with larger surface area during in-strokes is able to generate a higher efficiency.

4.2. Influence of surface area change ratio

For the variable surface area fin, two key parameters are concerned, the surface area change ratio and surface area change time. In Section 3, different surface area change ratios and time are defined, in this section, the influence of the surface area change ratio on the hydrodynamic response is firstly discussed and the experiment parameters are given in Table 3.

As shown in Fig. 12(a), the thrust forces of Mode III with various ratios are presented, which show similar force trajectories, but vary in amplitudes. Fin of ratio 1.2 generates the largest peaks and valley values and fin of ratio 1.4 shows the smallest amplitudes. The thrust forces of Mode IV are shown in Fig. 12(b). Fin of ratio 1.2 also generates the largest peaks but the difference between the two peaks increases compared to Mode III. Fin of ratio 1.4 generates the smallest valley values. We detailed calculate the average thrust force and efficiency as presented in Fig. 12(c). For the average thrust force, Mode III can generate more thrust force than Mode IV for all the three ratios, and possesses a negative linear relationship with the surface area change ratio. For Mode IV, the average thrust force increases with the decreasing of surface change ratio, but the slope

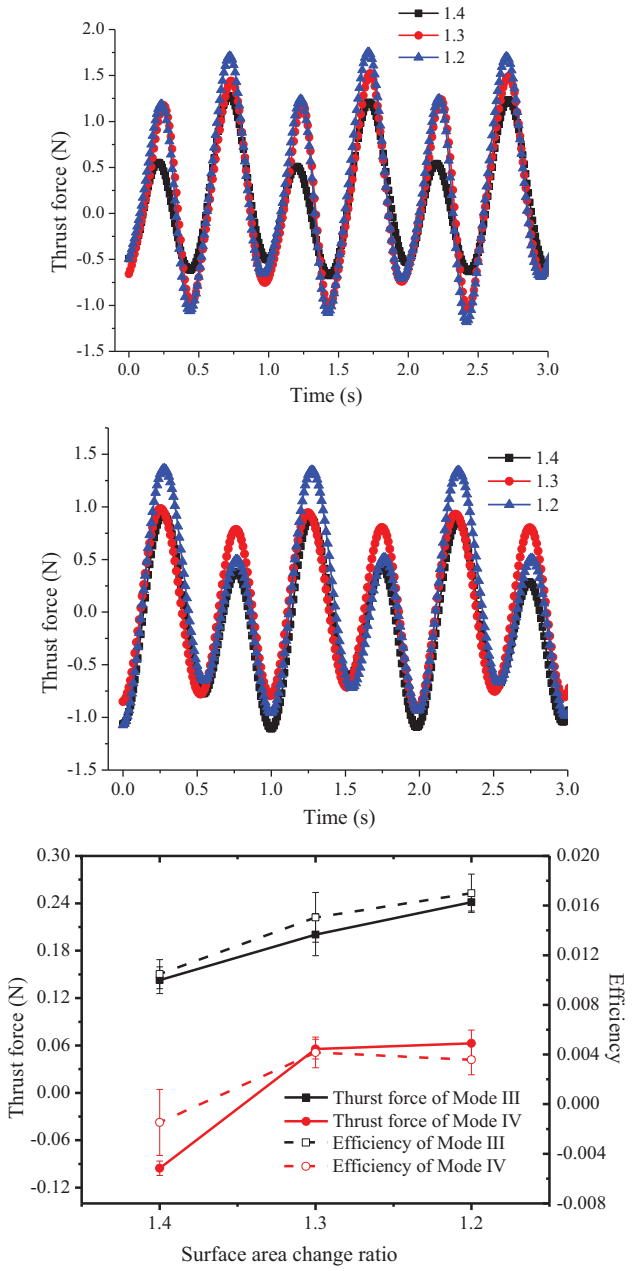

Fig. 12. Thrust force and efficieny of various surface area change ratios of Mode III and Mode IV, (a): thrust force of Mode III, (b): thrust force of Mode IV, (c): efficiency and average thrust force of the two modes.

ratio decreases when the ratio changes from 1.3 to 1.2. The efficiency of Mode III also increases with the decreasing of surface change ratio, and the efficiency of Mode IV firstly increases much as the ratio changes from 1.4 to ratio 1.3, and then decreases little for the ratio change from 1.3 to 1.2, which means there exists an optimal ratio to achieve the best efficiency.

4.3. Influence of surface area change time

The experiments to assess the surface area change time's effect are conducted with parameters listed in Table 4.

As shown in Fig. 13(a), the thrust forces in the case of surface area change time 0.05 s and 0.1 s are similar, while the force trajectories of surface area change time of 0.15 s exhibits much larger peaks. The forces for Mode IV are presented in Fig. 13(b), it is seen that

Table 4
Parameters used in experiment 3.

Parameter	Specific value
Pitching frequency	1 Hz
Pitching amplitude	45°
Swimming speed	0.25 L
Surface area change ratio	1.4
Surface area change time	0.05 s, 0.1 s, 0.15 s

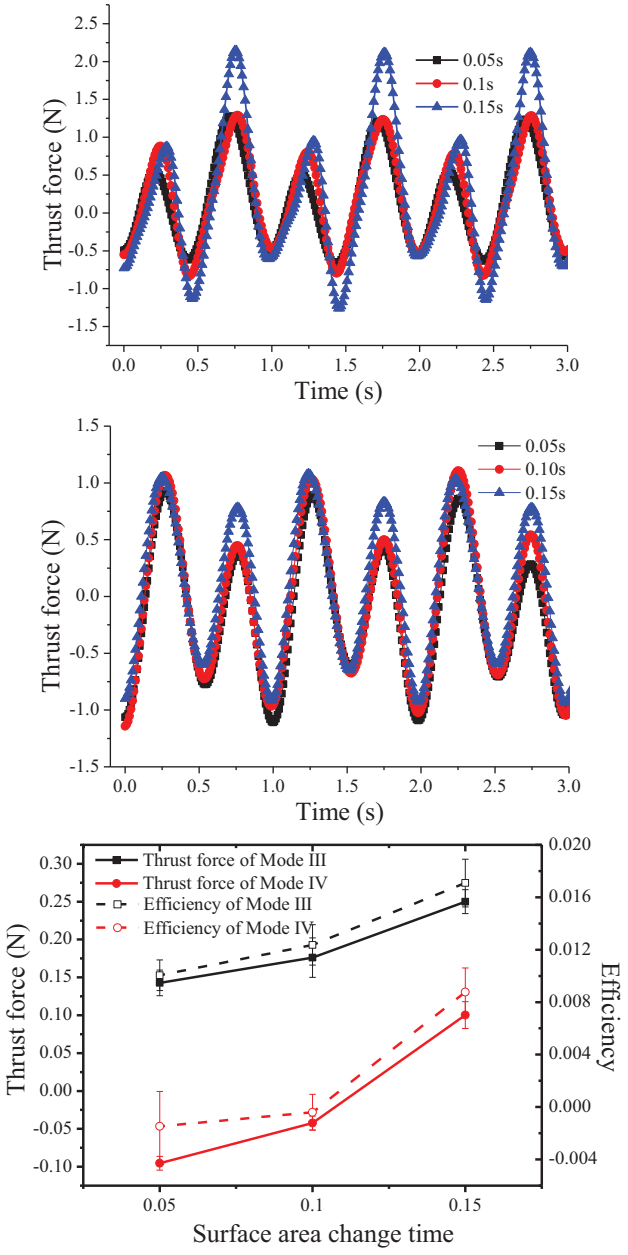

Fig. 13. Thrust force and efficiency of various surface area change time s of Mode III and Mode IV, (a): thrust force of Mode III, (b): thrust force of Mode IV, (c): efficiency and average thrust force of the two modes.

for the three surface change time the force trajectories show similar trends but vary in the peaks. The average thrust force and efficiency are exhibited in Fig. 13(c). Both the average thrust force of Mode III and Mode IV increase along with the surface area change time increasing, but the slop rates differ. The average thrust force increases larger when the change time increases from 0.1 s to 0.15 s than which

Table 5
Parameters used in experiment 4.

Parameter	Specific value
Pitching frequency	1 Hz, 0.75 Hz, 1.25 Hz
Pitching amplitude	45°, 30°, 60°
Swimming speed	0.25 L
Surface area change ratio	1.4
Surface area change time	0.05 s

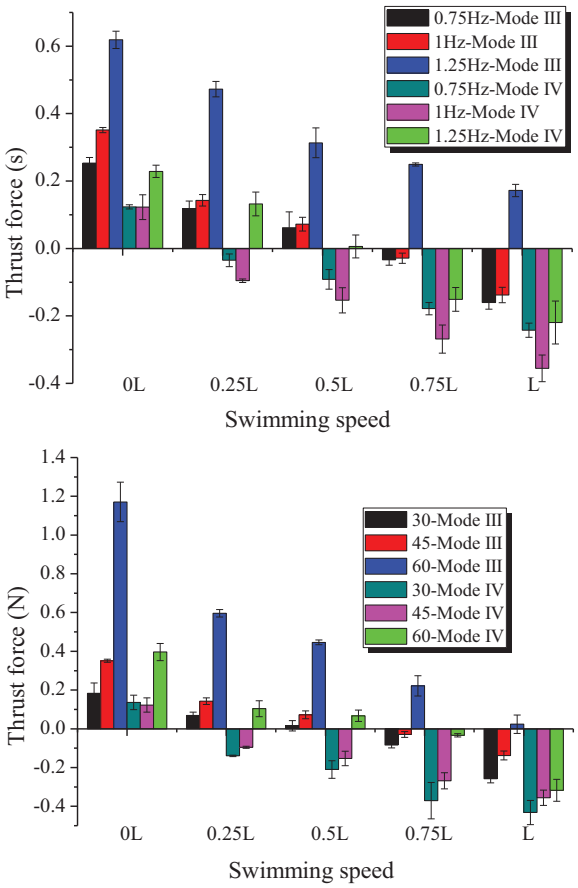

Fig. 14. Average thrust force of Mode III and Mode IV with different kinematic parameters. (a) pitching frequency, (b) pitching amplitude.

increases from 0.05 s to 0.1 s. Similarly, the efficiencies also increase with the change time increasing for both modes in our experiment.

4.4. Influence of kinematic parameters

Different kinematic parameters are adopted to assess their effects on Mode III and Mode IV. The parameters are presented in Table 5.

Different pitching frequencies are investigated as shown in Fig. 14(a). For Mode III, when the pitching frequency increases from 0.75 to 1 Hz, the average thrust force increases little for nearly all the swimming speeds. However, when the frequency increases from 1 to 1.25 Hz, the thrust force will increase sharply. It still can generate thrust force when the swimming speed is L mm/s while the other cases all generate drag forces. For Mode IV, the fin generates the largest force at frequency 1.25 Hz for all the speeds. However, when the frequency increases from 0.75 to 1 HZ, its average thrust force decreases, and when the swimming speed increases, the force difference increases too.

In Fig. 14 (b), the pitching amplitude's effect is analyzed. For Mode III, when the amplitude increases from 30° to 45°, the average thrust forces increase for all the speeds, and when the amplitude increases to 60°, the forces increase much larger. When the swimming speed is zero, the average thrust force reach 1.17 N. The forces for Mode IV are relatively smaller, but they also increase along with the amplitudes increasing.

4.5. Discussions

Fish fin possesses large deformations in its motion cycles to assist fish's swimming motion. Researchers come up with several basic motion patterns to describe the complex motion [19,20]. No matter in the "cupping" motion or "undulation" motion, the flapping surface area change is remarkable, let alone the "expanding" motion. Some researchers have conducted research on the surface area. Low studied the aspect ratio of flexible caudal fin [24] and Zhao investigated different shape of caudal fin [25] of which both of the surface area vary much, Tangorra *et al* designed pectoral and caudal fins whose surface area change dynamically in motion cycles which was affected by both of the 3D motions and fin's flexibility [26]. However, it is seen that their studies on surface area are indirectly and non-independent, the surface area change is either static which means no change in a transient cycle or is not the only variable, the surface area change are coupled with other parameters such as aspect ratio, fin flexibility, so they can't obtain the effect of dynamic surface area change in a motion cycle directly. In this paper, a novel robotic fin with dynamic variable surface area is focused while other parameters such as contours are fixed, by which way the hydrodynamic influence of dynamic surface area change can be analyzed independently. In our design, the surface area change is realized by rotating the cover fin to shield the holes in the base fin, it should be noticed that the fin prototype is different from the natural fish fin, since holes exist in our fin prototype. It is worth emphasizing that the purpose of the novel robotic fin is not to replicate fully the morphology of the fish fins but to verify the fluid effect of dynamic surface area change.

It is seen from the results that the dynamic surface area change indeed affects the fluid response prominently. For the four control modes of the surface area change introduced in this paper, two comparisons are conducted. Firstly, for the variable area fin, Mode III and Mode IV generate quite different force response compared with Mode I and Mode II and they generate average thrust forces between the complete fin (Mode I) and fin with smaller surface area (Mode II). However, for the efficiency, Mode III surpasses Mode I and generates the largest thrust efficiency. Secondly, between the two variable surface area fin, difference is obvious, the fin with larger surface during in-strokes can generate much larger average thrust force and efficiency than the fin with larger surface during out-strokes. The reason for the difference may lie in the complex coupling between the motion and vortex. The results indicate that the propulsive performance may be improved by proper dynamic surface area change. Mode III, namely, the fin with larger surface during in-strokes can generate the largest thrust efficiency with relatively large average thrust force, which may be a good choice for future underwater robotic propulsive system. More parameters are studied including the two key parameters of the surface area change and the pitching kinematic parameters. It is seen that their influences on the propulsive performance are closely related to the parameter values and control modes. To achieve a better performance of underwater propulsive system, these parameters should be chosen carefully to realize a positive coupling. It also should be noticed that the average thrust force and efficiency for swimming speed of 0.25 L is relatively small since the modes nearly achieve its cruise speed, we concentrate more attention on the comparative value than absolute value.

5. Conclusions

The paper proposes a novel design of variable area fish fin which is inspired by the fish fin's greatly deformation during swimming. A

base fin with hand shaped holes and a cover fin are designed, the cover fin can be driven to rotate to shield the holes easily to realize the fin surface area change which operates similar to close and open a window. Then a crank-rocker-cam composite mechanism is presented to realize the pitching motion and surface area change motion synchronously. Four control modes are presented and an experimental system is set up to measure the thrust force and efficiency. It is found out that the dynamic surface area change in a motion cycle generates giant influence on the hydrodynamic response. Mode III and Mode IV can generate average thrust force between Mode I and Mode II while Mode III's average thrust force is much larger than Mode IV. Meanwhile, Mode III can generate the largest thrust efficiency among the four modes. More features about the surface area change including the surface area change ratio and time are investigated. Meanwhile, the pitching kinematic parameters are detailed discussed. The results indicate that these parameters show a complicated coupling with the control modes and it can indeed improve the propulsive performance by choosing proper parameters. These results will be useful for the comprehensive understanding of the fin's complex deformations' effect on the hydrodynamic forces and can guide the design of novel underwater robotic propulsive system. In the future, more parameters of the fin's deformations such as its appearance contours, aspect ratio, sweepback will be investigated to obtain an overall understanding of the fin's motion and deformation.

Acknowledgment

This research has been financially supported by National Natural Science Foundation of China (no. 51375468, 50975270).

References

[1] Lightill MJ. Large-amplitude elongated-body theory of fish locomotion. Proc Roy Soc Lond B 1971;179:125–38.
[2] Wu TY. Hydromechanics of swimming propulsion. Part 1. Swimming of a two-dimensional flexible plate at variable forward speeds in an inviscid fluid. J Fluid Mech 1971;46:337–55.
[3] Byun D, Choi J, Cha K, Park J, Park S. Swimming microrobot actuated by two pairs of Helmholtz coils system. Mechatronics 2011;21:357–64.
[4] Wang JX, Tan XB. A dynamic model for tail-actuated robotic fish with drag coefficient adaptation. Mechatronics 2013;23:659–68.
[5] Abaid N, Bernhardt J, Frank JA, Kapila V, Kimani D, Porfiri M. Controlling a robotic fish with a smart phone. Mechatronics 2013;23(5):491–6.
[6] Lindsey CC. Form, function and locomotory habits in fish. In: Locomotion WS, Hoar, Randall DJ, editors. Fish Physiology, Vol. VII. New York: Academic; 1978. p. 1–100.
[7] Sfakiotakis M, Lane DM, Davies JBC. Review of fish swimming modes for aquatic locomotion. IEEE J Ocean Eng 1999;24:237–52.
[8] Westneat M, Thorsen DH, Walker JA, Hale M. Structure, function, and neural control of pectoral fins in fishes. IEEE J Ocean Eng 2004;29(3):674–83.
[9] Thorsen DH, Westneat MW. Diversity of pectoral fin structure and function in fishes with labriform propulsion. J Morphol 2005;263:133–50.
[10] Webb PW. Stability and maneuverability. Fish Biomechanics 2006;23:281–332.
[11] Rosenberger LJ, Westneat MW. Functional morphology of undulatory pectoral fin locomotion in the stingray taeniura lymma (chondrichthyes: dasyatidae). J Exp Biol 1999;202:3523–39.
[12] Rosenberger LJ. Pectoral fin locomotion in batoid fishes: undulation versus oscillation. J Exp Biol 2001;204:379–94.
[13] Yang SB, Qiu J, Han XY. Kinematics modeling and experiments of pectoral oscillation propulsion robotic fish. J Bionic Eng 2009;6(2):174–9.
[14] Low KH. Modeling and parametric study of modular undulating fin rays for fish robots. Mech Mach Theory 2009;44:615–32.
[15] Yan Q, Wang L, Liu B, Yang J, Zhang SW. A Novel Implementation of a Flexible Robotic Fin Actuated by Shape Memory Alloy. J Bionic Eng 2012;9:156–65.
[16] Lauder GV, Madden PGA, Mittal R, Dong H, Bozkurttas M. Locomotion with flexible propulsors: I. Experimental analysis of pectoral fin swimming in sunfish. Bioinsp Biomim 2006;1:s25–34.
[17] Lauder GV, Anderson EJ, Tangorra JL, Madden PGA. Fish biorobotics: kinematics and hydrodynamics of self-propulsion. J Exp Biol 2007;210(16):2767–80.
[18] Flammang BE, Lader GV. Caudal fin shape modulation and control during acceleration, braking and backing maneuvers in bluegill sunfish lepomis macrochirus. J Exp Biol 2009;212:277–86.
[19] Bozkurttas M, Mittal R, Dong H, Lauder GV, Madden GA. Low-dimensional models and performance scaling of a highly deformable fish pectoral fin. J Fluid Mech 2009;631:311–42.
[20] Wang L, Xu M, Liu B, Low KH, Yang J, Zhang SW. Three-Dimensional kinematics analysis of the Koi Carp pectoral fin by digital image processing. J Bionic Eng 2013;10(2):210–21.
[21] Tangorra JL, Lauder GV, Hunter IW, Mittal R, Madden PGA, Bozkurttas M. The effect of fin ray flexural rigidity on the propulsive forces generated by a biorobotic fish pectoral fin. J Exp Biol 2012;213:4043–54.
[22] Esposito CJ, Tangorra JL, Flammang BE, Lauder GV. A robotic fish caudal fin: effects of stiffness and motor program on locomotor performance. J Exp Bio 2012;215:56–67.
[23] Zhang SW, Liu B, Wang L, Yan Q, Low KH, Yang J. Design and implementation of a lightweight bioinspired pectoral fin driven by SMA. IEEE/ASME Trans Mechatronics 2014;19:1773–85.
[24] Low KH, Chong CW. Parametric study of the swimming performance of a fish robot propelled by a flexible caudal fin. Bioinsp Biomim 2010;5(4):046002.
[25] Zhao L, Jing J, Lu XY, Yin XZ. Measurements and analysis of force and moment of caudal fin model in C-start. Progress in Natural Science 2006;16(8):796–802.
[26] Tangorra J, Phelan C, Esposito C, Lauder G. Use of biorobotic models of highly deformable fins for studying the mechanics and control of fin forces in fishes. Int Comparative Bio 2011;1:176–89.